13th International Symposium on Particle Image Velocimetry – ISPIV 2019
Munich, Germany, July 22-24, 2019

Experimental study on fluid-structure interaction of a flexible membrane wing

Xi He[1], Jinjun Wang[1]*, Lihao Feng[1], Chong Pan[1]

[1]Beijing University of Aeronautics and Astronautics, Key Laboratory of Fluid Mechanics (Ministry of Education), Beijing, China

*jjwang@buaa.edu.cn

Abstract

A time-resolved particle image velocimetry (PIV) experiment was carried out to investigate the fluid-structure interaction (FSI) of a flexible membrane wing at a moderate angle of attack and low Reynolds numbers. The model was composed of a flexible membrane sheet and rigid leading/trailing edge supports. The dynamic characteristics of the membrane wing was firstly analyzed. While interacting with the fluid, the membrane would perform strongly periodic vibrations and present a shift of vibration modes with the increase of Reynolds number. The flow field was also captured in this study. It was found that the fluid-structure interaction played an important role in affecting the vortex shedding process over the wing surface.

1 Introduction

With the development of aviation, micro air vehicles (MAVs) are being applied for increasing purposes. As Shyy et al. (2005) indicated, MAVs have three prominent features: low Reynolds number ($10^4 \sim 10^5$), small physical dimensions and low flight speeds. These characteristics can result in degraded aerodynamic performance, intrinsically unsteady flight characteristics and sensitivity to the flight environments. The low Reynolds number flow regime was also characterized by low lift-to-drag ratio with problems of lift generation and flow attachment (Lissaman, 1983). However, it is required that these MAVs must have excellent aerodynamic efficiency and can adapt to different operating circumstances, such as gusts, ground effects, high angles of attack, variable temperature and density media. The controllability of these MAVs is also expected. Accordingly, promoting the aerodynamic performance of micro air vehicles has gradually become a great challenge.

Biological morphing-wing concept has been found to be important in the design of efficient MAVs, which is mainly because the sizes and operating conditions of MAVs are similar as natural flyers. The flexible membrane wings of bats were identified to be one of the essential features causing the aerodynamic superiority in maneuvering (Swartz et al. 2012). Considering the additional advantages of the membrane wings on reduced weight, high impact resistance and easier foldability (Bleischwitz 2016), it is worthwhile to investigate the aerodynamics of the membrane wings and their potential applications on MAVs.

Numerous works focused on membrane wings have been carried out in the past two decades. In the pioneering studies, Levin and Shyy (2001) attached a flexible membrane on the upper surface of a modified CLARK-Y airfoil and found the aerodynamic performance of the airfoil was improved with

such a passive control approach. Membrane wings were further observed to have unique advantages on delaying stall and adapting to the unsteady flight environment with the introduction in MAVs for sustained, robust and stable flight performance (Shyy et al. 2005). Subsequently, a fine pterosaur-like elasto-flexible morphing wing configuration was proposed and manufactured by Béguin et al. (2012). Flexible membranes were also used in their studies as aerodynamic surfaces for various planform geometries and airfoil shapes. It was shown that the passive membrane deflection combined with the active wing planform variation could effectively maintain high lift-to-drag ratios over a broad range of flight conditions. These studies mainly focused on applying flexible membrane wings on relatively complex configurations of MAVs, remaining the fundamental physical mechanisms to be solved.

Consequently, simplified membrane wings composed of a rigid support and a flexible wing surface were designed for fundamental research. Generally, there are three most common configurations of membrane wings in the literature: perimeter supported (Albertani et al. 2007; Rojratsirikul et al. 2011; Bleischwitz et al. 2016, 2017, 2018), batten supported (Albertani et al. 2007; Hu et al. 2008; Timpe et al. 2013) and leading/trailing supported (Galvao et al. 2006; Song et al. 2008; Rojratsirikul et al. 2009, 2010; Bleischwitz et al. 2015). Aerodynamic forces, dynamic characteristics and flow field of these membrane wings were investigated and a preliminary conclusion was drawn. Unlike the conventional rigid wings, membrane wings benefit a lot from their fluid-structure interaction characteristics (Gursul et al. 2014). The structures can passively deform and vibrate under the aerodynamic load, leading to camber changing. While in turn, the forces and the flow field are greatly influenced by the structural variations. However, few experimental studies have clarified the exact relationship between membrane vibration and vortex evolution, which is so-called fluid-structure coupling mechanism. As necessary for this aim, the time-resolved global flow fields as well as the time-synchronized membrane deformations are also rarely measured.

In this paper, a two-dimensional time-resolved (2D-TR) PIV was conducted for exploring the fluid-structure interaction of a membrane wing. The flow field and the membrane deformations were simultaneously captured. The full text is divided into following parts: introduction, experimental method, membrane dynamics, flow field and conclusion.

2 Experimental method

The present experiment was carried out in the low-speed, open-loop closed-jet wind tunnel at Beijing University of Aeronautics and Astronautics. The test section of the tunnel has a cross section of 42cm (width) × 50cm (height) with the free-stream turbulent intensity of about 0.3%. As shown in Fig. 1(a), the membrane wing was mounted in the test section through the leading/trailing edge supports and endplates. The tested angle of attack was α = 14º, which belongs to moderate angle of attack in the previous relevant works. The wing had a span of 360mm and chord length of c = 120mm. The free stream velocities U_∞ were in the range of 7.5 m/s ~ 10m/s, resulting in the Reynolds number based on c of $Re = 6\times10^4 \sim 8\times10^4$. The membrane wing illustrated in Fig. 1(b) was similar to the model of Bleischwitz et al. (2015), which was attached around 3mm round steel leading/trailing edges without pre-strain. The membrane was made from a transparent thermoplastic polyurethanes (TPU) sheet with a thickness of t = 0.2mm, Young's modulus of E = 31.2MPa and density of ρ = 1.1g/cm^3. The aeroelastic parameter is $\Pi = (Et/qc)^{1/3}$, which in this study had a value of Π = 15.1 ~ 9.5 for U_∞ = 7.5 m/s ~ 10m/s, respectively.

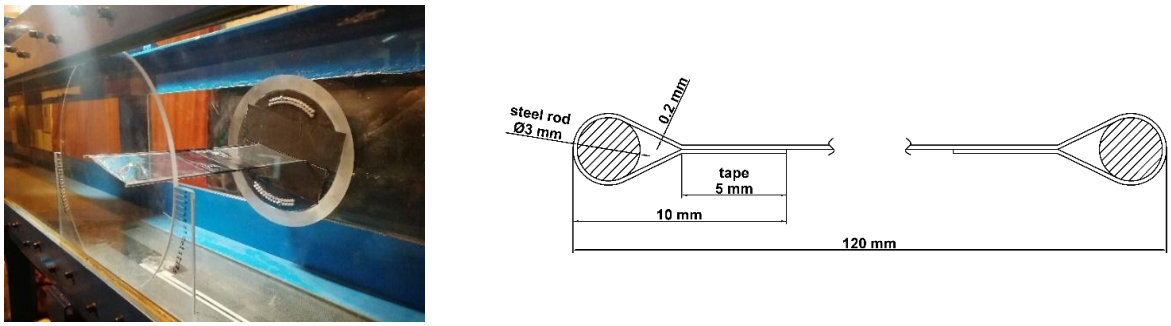

(a) Membrane wing in the test section (b) Details of membrane wing

Figure 1: Model installation.

PIV measurement was undertaken at the wing mid-span in a streamwise wing-normal plane. Illumination of the desired plane was achieved by using a Beamtech Vlite Hi-527 high-speed double-pulsed laser with a maximum energy of 30mJ/pulse at 1 kHz frame rate. The thickness of the laser sheet was approximately 1mm. A Photron Fastcam SA2/86K-M3 high-speed CMOS camera was placed normal to the flow to capture image pairs. The laser and the camera were synchronized by a MicroVec Micropulse 725 synchronizer. The sampling speed was set to 1 kHz at a spatial resolution of 1024 × 800 pixels, producing sequences of 14000 instantaneous velocity fields over 14 seconds. Glycerol-water mixture droplets with a mean size of about 1μm were generated and seeded by an AG 1500W fog machine as tracer particles. The raw images were processed based on the multi-pass iterative Lucas-Kanade algorithm (MILK) accelerated by GPU (Pan et al. 2015) to obtain original velocity fields. The interrogation window size was set to 32 × 32 pixels with a 75% overlap.

3 Membrane dynamics

The dynamic characteristics of the membrane wing which could be extracted from the membrane deformations were firstly analyzed. The mean and instantaneous membrane profiles at α = 14º are shown in Fig. 2(a), (b) and (c). The standard deviations of the vertical membrane motions z_{std} (see Eq. 1) are presented in Fig. 2(d). It can be observed that the first-order, second-order and third-order modes are dominant vibration modes at each *Re* respectively. The mode number of the membrane wing increases with *Re*, which is consistent with previous observations of Rojratsirikul et al. (2009). It is also found in Fig. 2 that the maximum camber of the membrane wing slightly increases with *Re*. This is because the increasing *Re* leads to the increase of pressure difference between the upper and lower wing surfaces and thus causes greater membrane deformation.

$$z_{std}(x,y) = \sqrt{\frac{1}{T}\sum_{t=0}^{T}(z(x,y,t) - \bar{z}(x,y))^2} \quad (1)$$

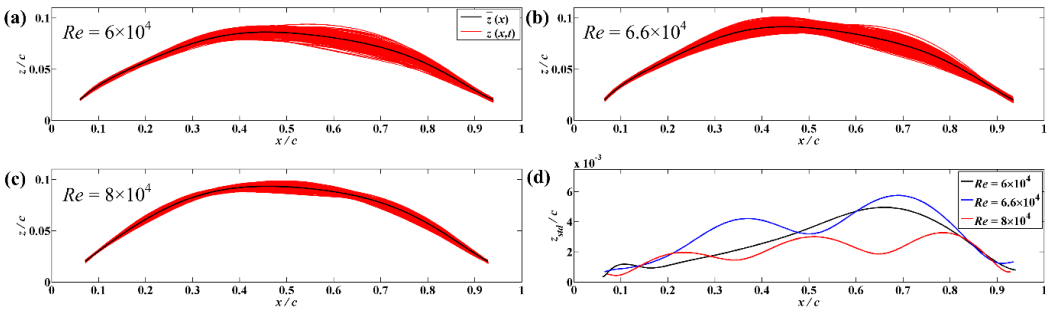

Figure 2: Membrane dynamics. (a) Re = 6×10⁴; (b) Re = 6.6×10⁴; (c) Re = 8×10⁴; (d) Standard deviations of the vertical membrane motions.

4 Flow field

As for the flow field, the statistical characteristics were investigated. Normalized time-averaged velocity ($\sqrt{U^2+V^2}/U_\infty$) as well as the time-averaged streamlines are shown in Fig. 3(a). It can be seen that there exists a recirculation region over the membrane wing surface near the trailing edge at Re = 6×10⁴, where the membrane presents a first-order-dominant vibration mode. The size of the recirculation region greatly decreases and basically disappears at Re = 6.6×10⁴, where the membrane presents a second-order-dominant vibration mode. However, a recirculation region appears downstream the trailing edge at Re = 8×10⁴, where the membrane presents a third-order-dominant vibration mode. The differences of the size and position of recirculation region among these Re cases may result from the fluid-structure interaction. Fig. 3(b) shows the normalized time-averaged vorticity ($\omega c/U_\infty$). The negative and positive value regions indicate the shear layers of the leading edge and trailing edge, respectively. With the increase of Re, the shear layer at the wing leeward side shows a tendency to approach the membrane wing surface.

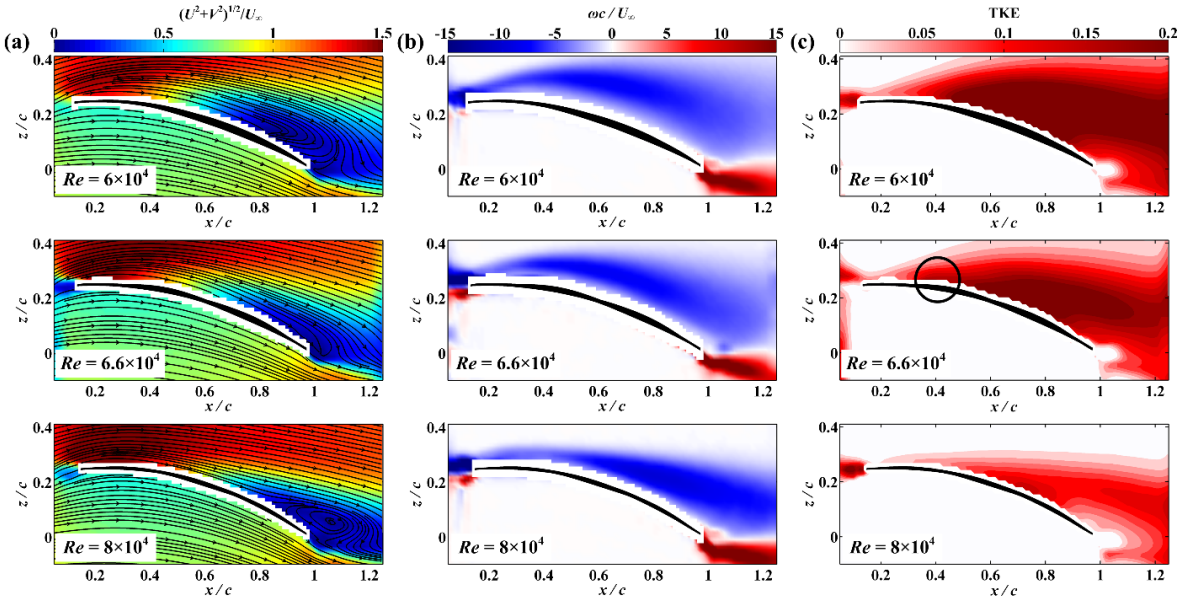

Figure 3: Membrane dynamics. (a) Time averaged velocity and streamlines; (b) Time averaged vorticity; (c) Turbulent kinetic energy.

Moreover, the normalized turbulent kinetic energy ($\overline{u'^2 + v'^2}/U_\infty^2$), TKE, is presented in Fig. 3(c). Membrane wings are found to exhibit strong velocity fluctuations over the wing surface and very weak velocity fluctuations below the wing surface. Similarly, the tendency of the shear layer to approach the wing surface with *Re* increasing can be discovered. Besides, comparing with *Re* = 6×10⁴ case, there seems to be another TKE concentrated region at a more upstream position at *Re* = 6.6×10⁴ (marked with the black circle). Considering the second-order-dominant vibration mode at this *Re*, it can be deduced that the membrane vibration and the velocity fluctuations have a close relationship due to the fluid-structure interaction.

Frequency characteristics of the time-resolved flow fields and membrane motions were further studied. The vibration of the membrane wing as well as the flow field were found to be quasi-periodic. Hence, Fourier mode decomposition (FMD) (Ma et al. 2015) was adopted to analyze the relationship between the membrane wing and the flow. The frequency spectra of the global flow field and membrane are plotted in Figure 4. It is clear that the membrane vibrations present obvious dominant frequency peaks in all *Re* cases. Specifically, 35.1Hz, 69.7Hz and 108Hz for the first–order, second-order and third-order dominant mode cases. 69.7Hz and 108Hz seem to be the double and triple frequencies of 35.1Hz.

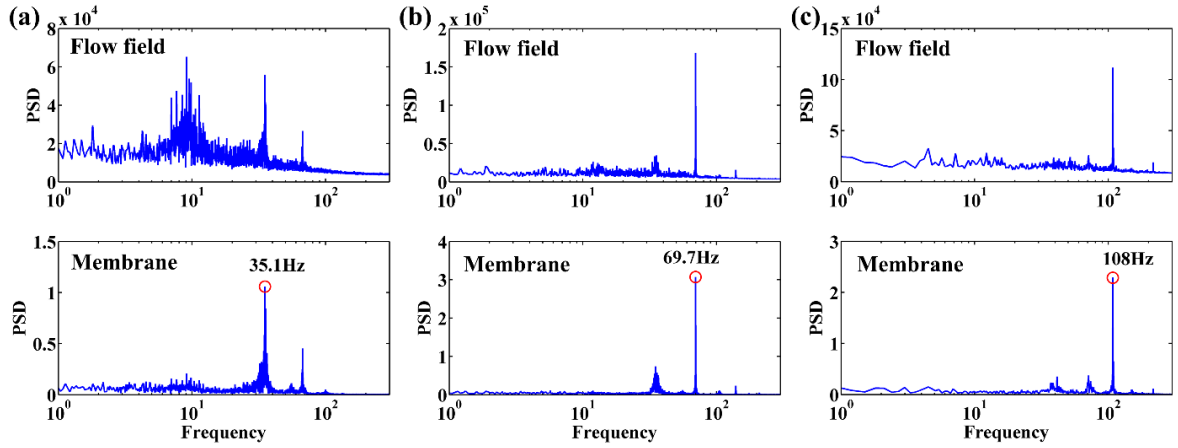

Figure 4: Frequency spectra of the global flow field and membrane. (a) *Re* = 6×10⁴; (b) *Re* = 6.6×10⁴; (c) *Re* = 8×10⁴.

The vibration frequencies of the membrane wing are strongly related to the global flow field spectra. In Fig. 4(b) and (c), the global flow field spectra show a similarity with the membrane vibration spectra. They both have identical and obvious dominant frequencies while the lower frequency contributions to the spectra are relatively small. The consistence of the dominant frequency between the global flow field and the membrane wing means the flow and the membrane vibration reach a coupling state. The vibration frequency of the membrane wing is also accurately reflected in the global flow field spectra in Fig. 4(a). However, the dominant frequency of the flow field is located at a much lower frequency around 9Hz. The possible reason for this frequency is the occurrence of vortex merging.

The dynamic Fourier modes corresponding to the membrane vibration frequencies could be obtained by FMD method and are presented in Figure 5. These Fourier modes based on vertical velocities mainly present vortex shedding processes in the shear layer at the wing leeward side. Considering the high contributions of the membrane vibration frequencies in the flow field spectra, the dominant

feature of the flow is the vortex shedding over the wing surface. As shown, the size of the Fourier mode and the distance between adjacent structures gradually reduce with the increase of *Re*. Besides, it should be noticed that the wavelength of membrane vibration also decreases due to the shift of vibration mode with the increase of *Re*. The consistence of the wavelength between the vortex structures and membrane vibration further indicates a fluid-structure coupling state.

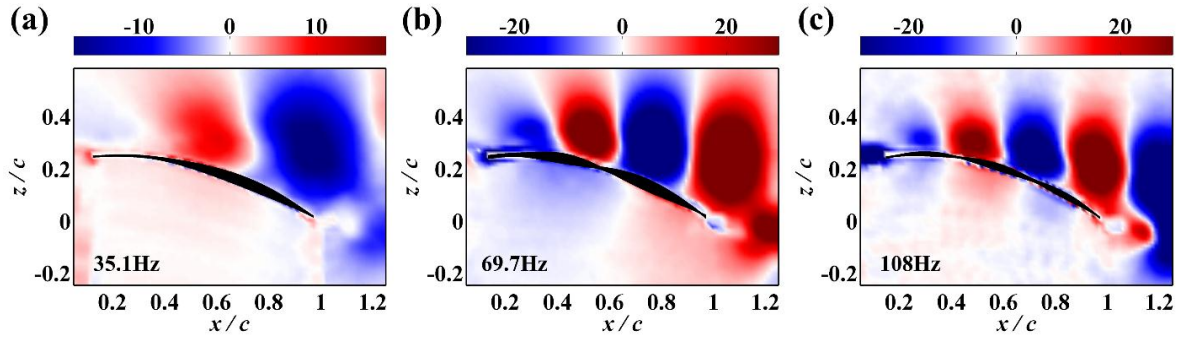

Figure 5: Global Fourier modes based on vertical velocities. (a) $Re = 6\times10^4$; (b) $Re = 6.6\times10^4$; (c) $Re = 8\times10^4$.

5 Conclusion

This paper experimentally discussed the fluid-structure interaction of a flexible membrane wing at a moderate angle of attack. With the increase of *Re*, the camber of the membrane wing slightly increased while the vibration modes shifted from first-order-dominant mode to third-order-dominant mode. The membrane vibration could enhance the velocity fluctuations over the wing surface, which had a significant influence on the flow field. The dominant frequencies of the flow fields and the vortex shedding processes were greatly changed with the shift of vibration modes due to the fluid-structure interaction.

Acknowledgements

This work was supported by the National Natural Science Foundation of China (No. 11761131009 and 11721202).

References

Shyy W, Ifju PG, and Viieru D (2005) Membrane wing-based micro air vehicles. *Applied Mechanics Reviews* 58(7):283-301

Lissaman PBS (1983) Low-Reynolds-number airfoils. *Annual Review of Fluid Mechanics* 15:223-239

Swartz SM, Iriarte-Diaz J, Riskin DK, and Breuer KS (2012) A bird? A plane? No, it's a bat: an introduction to the biomechanics of bat flight. *Evolutionary History of Bats: Fossils, Molecules and Morphology*. Chapter 9, pages 317-351. Cambridge University Press, evolution edition

Bleischwitz R (2016) Fluid-structure interactions of membrane wings in free-flight and in ground-effect. University of Southampton, Faculty of Engineering and the Environment, Doctoral Thesis

Levin O, and Shyy W (2001) Optimization of a low Reynolds number airfoil with flexible membrane. *Cmes-Computer Modeling in Engineering and Sciences* 2(4):523-536

Béguin B, Breitsamter C, and Adams N (2012) Aerodynamic investigations of a morphing membrane wing. *AIAA Journal* 50(11):2588 – 2599

Albertani R, Stanford B, Hubner J, and Ifju P (2007) Aerodynamic coefficients and deformation measurements on flexible micro air vehicle wings. *Experimental Mechanics* 47:625-635

Rojratsirikul P, Genc MS, Wang Z, and Gursul I (2011) Flow-induced vibrations of low aspect ratio rectangular membrane wings. *Journal of Fluids and Structures* 27:1296-1309

Bleischwitz R, de Kat R, and Ganapathisubramani B (2016) Aeromechanics of membrane and rigid wings in and out of ground-effect at moderate Reynolds numbers. *Journal of Fluids and Structures* 62:318-331

Bleischwitz R, de Kat R, and Ganapathisubramani B (2017) On the fluid-structure interaction of flexible membrane wings for MAVs in and out of ground-effect. *Journal of Fluids and Structures* 70:214-234

Bleischwitz R, de Kat R, and Ganapathisubramani B (2018) Near-wake characteristics of rigid and membrane wings in ground-effect. *Journal of Fluids and Structures* 80:199-216

Hu H, Tamai M, and Murphy T (2008) Flexible-membrane airfoils at low Reynolds numbers. *Journal of Aircraft* 45(5):1767-1778

Timpe A, Zhang Z, Hubner J, and Ukeiley L (2013) Passive flow control by membrane wings for aerodynamic benefit. *Experiments in Fluids* 54(3):1471

Galvao R, Israeli E, Song A, Tian X, Bishop K, Swartz S, and Breuer K (2006) The aerodynamics of compliant membrane wings modelled on mammalian flight mechanics. In *36th AIAA Fluid Dynamics Conference and Exhibit, San Francisco, California, USA, June 5-8*

Song A, Tian X, Israeli E, Galvao R, Bishop K, Swartz S, and Breuer K (2008) Aeromechanics of membrane wings with implications for animal flight. *AIAA Journal* 46(8):2096-2106

Rojratsirikul P, Wang Z, and Gursul I (2009) Unsteady fluid-structure interactions of membrane airfoils at low Reynolds numbers. *Experiments in Fluids* 46:859-872

Rojratsirikul P, Wang Z, and Gursul I (2010) Effect of pre-strain and excess length on unsteady fluid-structure interactions of membrane airfoils. *Journal of Fluids and Structures* 26:359-376

Bleischwitz R, de Kat R, and Ganapathisubramani B (2015) Aspect-ratio effects on aeromechanics of membrane wings at moderate Reynolds numbers. *AIAA Journal* 53(3):780-788

Gursul I, Cleaver DJ, and Wang Z (2014) Control of low Reynolds number flows by means of fluid–structure interactions. *Progress in Aerospace Sciences* 64:17-55

Pan C, Xue D, Xu Y, Wang JJ, and Wei RJ (2015) Evaluating the accuracy performance of Lucas-Kanade algorithm in the circumstance of PIV application. *Science China Physics Mechanics and Astronomy* 58(10):1-16

Ma LQ, Feng LH, Pan C, Gao Q, and Wang JJ (2015) Fourier mode decomposition of PIV data. *Science China Technological Sciences* 58:1935-1948